

Structural, electronic, and Li-ion mobility properties of garnet-type $Li_7La_3Zr_2O_{12}$ surface: An insight from first-principles calculations

Jing-Xuan Wang(王靖轩), Bao-Zhen Sun(孙宝珍), Mei Li(李梅), Mu-Sheng Wu(吴木生), and Bo Xu(徐波)
Citation: Chin. Phys. B, 2023, 32 (**6**): 068201. DOI: 10.1088/1674-1056/acc05d
Journal homepage: http://cpb.iphy.ac.cn; http://iopscience.iop.org/cpb

What follows is a list of articles you may be interested in

Stress effect on lattice thermal conductivity of anode material $NiNb_2O_6$ for lithium-ion batteries

Ao Chen(陈奥), Hua Tong(童话), Cheng-Wei Wu(吴成伟), Guofeng Xie(谢国锋), Zhong-Xiang Xie(谢忠祥), Chang-Qing Xiang(向长青), and Wu-Xing Zhou(周五星)
Chin. Phys. B, 2023, 32 (**5**): 058201. DOI: 10.1088/1674-1056/acaa2d

Tailoring of thermal expansion and phase transition temperature of ZrW_2O_8 with phosphorus and enhancement of negative thermal expansion of $ZrW_{1.5}P_{0.5}O_{7.75}$

Chenjun Zhang(张晨骏), Xiaoke He(何小可), Zhiyu Min(闵志宇), and Baozhong Li(李保忠)
Chin. Phys. B, 2023, 32 (**4**): 048201. DOI: 10.1088/1674-1056/ac9364

Liquid-phase synthesis of Li_2S and Li_3PS_4 with lithium-based organic solutions

Jieru Xu(许洁茹), Qiuchen Wang(王秋辰), Wenlin Yan(闫汶琳), Liquan Chen(陈立泉), Hong Li(李泓), and Fan Wu(吴凡)
Chin. Phys. B, 2022, 31 (**9**): 098203. DOI: 10.1088/1674-1056/ac7459

First-principles insight into Li and Na ion storage in graphene oxide

Shu-Ying Zhong(钟淑英), Jing Shi(石晶), Wen-Wei Luo(罗文崴), Xue-Ling Lei(雷雪玲)
Chin. Phys. B, 2019, 28 (**7**): 078201. DOI: 10.1088/1674-1056/28/7/078201

A high-performance rechargeable Li-O_2 battery with quasi-solid-state electrolyte

Jia-Yue Peng(彭佳悦), Jie Huang(黄杰), Wen-Jun Li(李文俊), Yi Wang(王怡), Xiqian Yu(禹习谦), Yongsheng Hu(胡勇胜), Liquan Chen(陈立泉), Hong Li(李泓)
Chin. Phys. B, 2018, 27 (**7**): 078201. DOI: 10.1088/1674-1056/27/7/078201

Structural, electronic, and Li-ion mobility properties of garnet-type $Li_7La_3Zr_2O_{12}$ surface: An insight from first-principles calculations

Jing-Xuan Wang(王靖轩)[1], Bao-Zhen Sun(孙宝珍)[1,2,†], Mei Li(李梅)[1], Mu-Sheng Wu(吴木生)[1], and Bo Xu(徐波)[1,‡]

[1] *Department of Physics, Laboratory of Computational Materials Physics, Jiangxi Normal University, Nanchang* 330022, *China*
[2] *Institute of Advanced Scientific Research (iASR) & Key Laboratory of Functional Small Molecules for Ministry of Education, Jiangxi Normal University, Nanchang* 330022, *China*

(Received 13 December 2022; revised manuscript received 29 January 2023; accepted manuscript online 2 March 2023)

Garnet-type $Li_7La_3Zr_2O_{12}$ (LLZO) is a promising solid-state electrolyte for Li-ion batteries, but Li-dendrite's formation greatly limits the applications. In this paper, we systematically investigate the stability, electronic properties, and Li-ion mobility of the LLZO surface by the first-principles calculations. We consider the (110) and (001) slab structures with different terminations in the t- and c-LLZO. Our results indicate that both (110) and (001) surfaces prefer to form Li-rich termination due to their low surface energies for either t- or c-LLZO. Moreover, with the decrease of Li contents the stability of Li-rich surfaces is improved initially and degrades later. Unfortunately, the localized surface states at the Fermi level can induce the formation of metallic Li on the Li-rich surfaces. In comparison, Li/La-termination has a relatively low metallic Li formation tendency due to its rather low diffusion barrier. In fact, Li-ion can spontaneously migrate along path II (Li3 → Li2) on the Li/La–T(001) surface. In contrast, it is more difficult for Li-ion diffusion on the Li–T(001) surface, which has a minimum diffusion barrier of 0.50 eV. Interestingly, the minimum diffusion barrier decreases to 0.34 eV when removing four Li-ions from the Li–T(001) surface. Thus, our study suggests that by varying Li contents, the stability and Li-ion diffusion barrier of LLZO surfaces can be altered favorably. These advantages can inhibit the formation of metallic Li on the LLZO surfaces.

Keywords: solid-state electrolyte, $Li_7La_3Zr_2O_{12}$ (LLZO) surface, Li-ion migration, first-principles calculations

PACS: 82.47.Aa, 71.15.Mb, 61.66.Fn, 68.35.Md **DOI:** 10.1088/1674-1056/acc05d

1. Introduction

Lithium-ion batteries (LIBs) are widely used in electric vehicles, grid storage equipment, etc.[1,2] With the development of society, higher requirements are put forward on the performance of batteries, and it is necessary to develop batteries with high safety performance and high energy density.[3,4] Traditional Li-ion batteries often use graphite as the anode material, and the theoretical capacity of graphite is 372 mAh/g. In order to meet people's needs and further improve the energy density of the battery to more than 300 Wh/kg, Li metal is the right choice as the anode. Li metal anode, in which the theoretical capacity of 3860 mAh/g is ten times larger than that of graphite with the lowest electrode potential (−3.04 V vs. standard hydrogen electrode), is an ideal negative electrode for LIBs.[5] In the past decades, the traditional battery electrolyte has been an organic liquid electrolyte. However, the liquid electrolyte is flammable, volatile, and easily punctured by the generated Li dendrites to cause a short circuit.[6–9] Moreover, the liquid electrolyte undergoes a liquid–solid transformation at low temperatures, and the ionic conductivity is significantly reduced. Obviously, these limit the safety, long cycle life, and environmental cleanliness of LIBs.[10,11] Compared with liquid electrolytes, solid-state electrolytes (SSE) use nonflammable inorganic solid materials with advantages, such as excellent safety properties and low electronic conductivity.[12] Since the Li-stuffed garnet-type $Li_7La_3Zr_2O_{12}$ (LLZO) exhibits excellent stability toward Li metal, wide electrochemical stability window (∼ 6 eV),[13] and modestly high ionic conductivity (t-LLZO about 10^{-6} S·cm^{-1} and c-LLZO about 10^{-4} S·cm^{-1} at room temperature), LLZO is regarded as a promising solid-state electrolyte for the next-generation solid-state Li batteries.[14–16] Despite the benefits, the problem of Li dendrites formed at the surface or interface is still an urgent problem to be solved for LLZO.

So far, people have realized that the Li dendrite growth is closely related with the grain boundaries, surfaces, voids and cracks in SSE. Therefore, modification of these defect sites is proposed to suppress the Li dendrite growth. Experimentally, a solid-state electrolyte interphase (SEI)-like interfacial layer between Li and SSE is used to alleviate the growth of dendritic Li.[17] Microstructural aspects, such as grain size, could affect mechanical and electrochemical properties, thereby changing the critical current density for Li plating.[18] By flatting the surface of the LLZO pellets and using buffer to improve the contact between LLZO and Li electrodes, the interface resistance could be dramatically reduced, which prevents the Li dendrite growth when running the same current through the cells.[19] The fact that Li_2CO_3 and LiOH formed on the sur-

†Corresponding author. E-mail: bzsun@jxnu.edu.cn
‡Corresponding author. E-mail: bxu4@mail.ustc.edu.cn

© 2023 Chinese Physical Society and IOP Publishing Ltd

face can efficiently fill the voids, which is advantageous in suppressing the growth of lithium dendrites.[20] Although the growth of Li dendrites is alleviated to a certain extent experimentally, this problem has not been solved completely. Especially, the fundamental origin and evolution of Li dendrite growth along the grain boundaries or defective sites of garnet LLZO are unclear, thus hindering the development of practical solid-state batteries with Li metal anode.

We know that the growth of Li dendrites requires the presence of conductive electrons and Li-ions. Reducing the electronic conductivity of SSE, and increasing the ionic conductivity can suppress the growth of Li dendrites. Several experimental and theoretical studies have improved the ionic conductivity of SSE by different atomic doping over the past years.[21–26] For example, Li-ion conductivities can be enhanced significantly for Al-doped LLZO,[22] Ga-doped LLZO,[21] Al^{3+} and Ga^{3+} co-doped LLZO,[27] and Ta-doped LLZO.[23,28] In these cases, doping does not greatly alter the topology of the migration pathway, but instead creates Li^{+} vacancies. As a result, the Li concentration within the surfaces or grain boundaries will vary accordingly, which further affects the formation of metallic Li. However, the information of the LLZO surface with different Li concentrations is missing. Furthermore, although the Li-ion transport properties in the bulk are clearly illustrated,[29,30] the Li-ion diffusion on the surface is unclear.

Motivated by the above considerations, in this paper, we systematically studied the structural, electronic, and ion diffusion properties of the LLZO surface by using the first-principles calculations based on the density functional theory (DFT). The (110) and (001) surfaces of t-LLZO and c-LLZO were considered. In particular, the effect of Li concentration on the thermodynamic stability and Li-ion mobility of the LLZO surfaces was also evaluated. Our study would provide the further understanding of electronic and ionic situation of the LLZO surface, which is closely related with the formation of Li metal within the surfaces or grain boundaries.

2. Computational details

In this paper, all calculations were performed by using the Vienna *ab initio* simulation package (VASP),[31] which is based on the density functional theory (DFT). The valence electron and core ion interaction were described by the projected-augmented wave (PAW) method.[32] The exchange–correlation energy was described with the generalized gradient approximation (GGA)[33] and the Perdew–Burke–Ernzerhof (PBE)[34] functional. The valence electron configurations of Li, La, Zr, and O atoms were $2s^1 2p^0$, $5d^1 6s^2$, $4d^2 5s^2$, and $2s^2 2p^4$, respectively. The cutoff energy of the plane wave was set to 550 eV, and the energy and force convergence were set to 10^{-5} eV per unit cell and 0.02 eV/Å, respectively. The Monkhorst–Pack method[35,36] with $2\times2\times2$ k-point grid mesh for the structural relaxations and $3\times3\times3$ k-point grid mesh for the electronic structure calculations were employed for the integration in the irreducible Brillouin zone of LLZO bulk crystals. For the surface configurations, $2\times2\times1$ and $3\times3\times1$ k-point grids were used for the structural relaxations and electronic structure calculations, respectively. A vacuum space of 20 Å was used to prevent the interaction between the atoms of the adjacent slabs.

The surface energy of the slab configurations with different termination planes was determined by the following expression:

$$\gamma = \frac{1}{2S}\left(E_{\text{slab}} - n_{\text{formula}}\mu_{\text{bulk}} - \sum n_i\mu_i\right), \tag{1}$$

where S is the surface area of the slab, E_{slab} is the total energy of the slab, n_{formula} is the integer number of stoichiometric formula units in the slab, μ_{bulk} is the energy of one formula unit of bulk LLZO, n_i is the number of atoms with type i in the slab in excess of the stoichiometric amount. μ_i is the chemical potential of element i, the values used in this work are from the DFT research of Thompson *et al*.[13]

In addition, the climbing image nudged elastic band (CI-NEB)[37] method was used to search the migration path and evaluate the migration barrier of Li-ion on the LLZO surface, which is an efficient method to find the energy saddle points for the Li-ion transition.[38] The calculation workflow was managed by the high-throughput computational platform for battery materials.[39]

3. Results and discussion

3.1. Bulk atomic and electronic structures

3.1.1. Bulk atomic structure

We firstly address the LLZO bulk structures and electronic properties separately. Garnet-type LLZO has two different crystal phases, namely, tetragonal LLZO (t-LLZO) and cubic LLZO (c-LLZO).[14] According to the experimental results,[40,41] we construct the crystalline models of t-LLZO and c-LLZO. Either of them contains 192 atoms in one unit cell, and meets with the stoichiometric formula $Li_7La_3Zr_2O_{12}$. The t-LLZO structure belongs to the space group $I4/acd$ (No. 142) with lattice parameters of $a = b = 13.13$ Å, and $c = 12.67$ Å. Figure 1 displays the distribution of Li-ions and the loop arrangement of different Li sites in the t-LLZO and c-LLZO. As shown in Fig. 1(a), there are three kinds of Wyckoff sites to accommodate Li-ions, which are the tetrahedral 8a (Li1) sites, the different distorted octahedral 16f (Li2) and 32g (Li3) sites. In this structure, Li crystallographic sites are fully occupied.[41]

The c-LLZO structure belongs to the space group $Ia\bar{3}d$ (No. 230) with lattice parameters of $a = b = c = 12.98$ Å. Two different Li sites, a tetrahedral 24d (Li1) site and a distorted

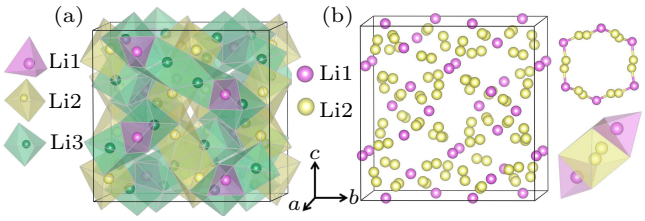


Fig. 1. Three-dimensional network structures of the Li atomic arrangement in (a) t-LLZO and (b) c-LLZO.

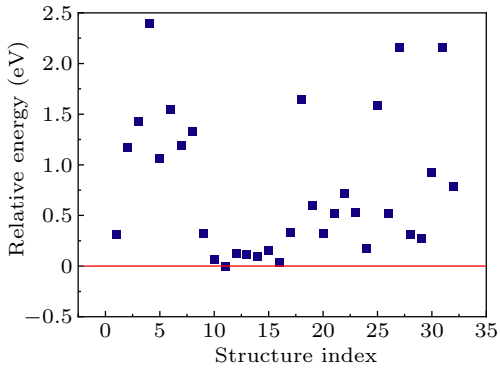


Fig. 2. Calculated relative energies of c-LLZO with different Li distribution.

octahedral 96h (Li2) site,[40] have been identified. Actually, the main difference between t-LLZO and c-LLZO lies in the occupancy of Li-ions. As mentioned above, Li-ions are fully occupied in the t-LLZO. In the c-LLZO, however, Li-ions are partially occupied on the 24d and 96h sites. There are 120 possible Li sites in the c-LLZO unit cell, as shown in Fig. 1(b). Specifically, the sites of Li in the c-LLZO structure are loop connections, and the connection order is Li1–Li2–Li2–Li1. According to the stoichiometric formula $Li_7La_3Zr_2O_{12}$, only 56 Li sites are occupied in the unit cell. Since the distance between two adjacent Li2 on the 96h sites (0.77 Å) is too small, the adjacent Li2 sites could not be occupied by Li-ions simultaneously due to the significant Coulomb repulsion interaction between them. Awaka *et al.*[41] found an occupancy of almost one ($g = 0.94$) of the 24d sites and a considerably reduced site occupancy ($g = 0.35$) of the 96h sites. Alternatively, the results observed by the neutron diffraction method with the occupancy rate of 24d sites ($g = 0.56$) and 96h sites ($g = 0.44$) were reported.[42] In addition, one principle about Li distribution should be considered. The Li1–Li2–Li1 connection order needs to be broken as the uniform vacancy distribution is beneficial to the diffusion of Li-ions.[42] Therefore, Li-ions are randomly distributed over 24d (Li1) and 96h (Li2) according to the above two different Li1/Li2 proportions. In this context, 32 configurations of c-LLZO with different Li distribution are chosen for the energy calculations. Taking the lowest-energy structure as a reference, the relative energies for these structures are shown in Fig. 2. Among them, the configuration with the lowest energy (see Fig. S1 in the supplementary material) has been adopted as the representative structure of c-LLZO.

3.1.2. Bulk electronic structure

As we all know, an important property to evaluate SSE is the electrochemical window, which describes the ability to suppress electron conduction in SSE. Fast ion-conducting solid-state electrolytes should exhibit enough broad electrochemical window to resist electron transport and remain stable. Basically, the band gaps of the SSE materials could be used to reflect the electrochemical window approximatively. Therefore, we obtain the bandgap from the calculated density of states (DOS) for both t-LLZO and c-LLZO. The calculated results are analyzed and plotted in Fig. 3. The bandgaps of t-LLZO and c-LLZO are about 4.1 eV and 4.0 eV, respectively. Generally, the GGA method underestimates the band gap. In a previously published study,[13] undoped c-LLZO band gaps calculated at the HSE06, PBE + GW and HSE06 + G0W0 levels are approximately 5.80 eV, 6.07 eV, and 6.42 eV, respectively. Although the bandgaps are significantly underestimated, LLZO exhibits a wide electrochemical window and blocks electron conductance effectively. According to the partial DOS of each atom, the valence band parts mainly result

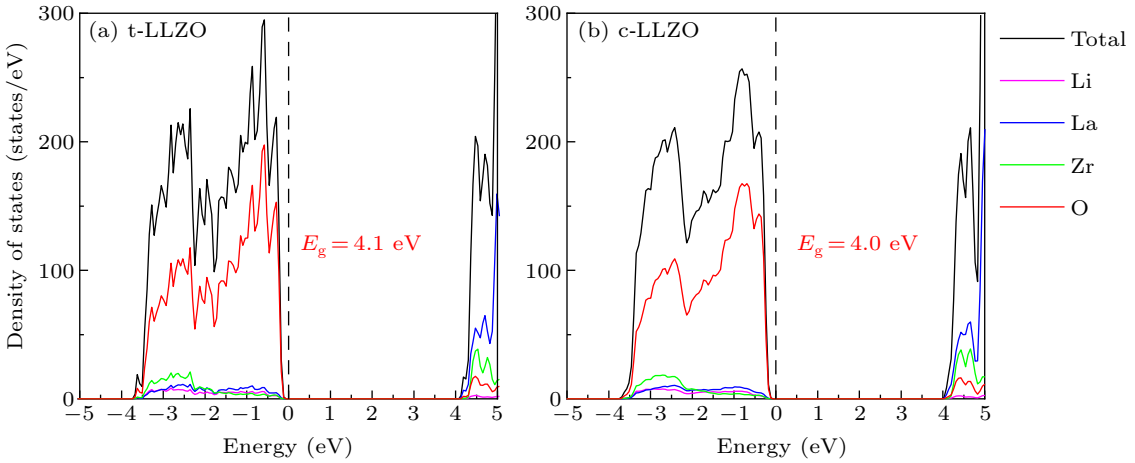


Fig. 3. Calculated total and partial density of states (DOS) using the PBE method for the (a) t-LLZO and (b) c-LLZO bulk structures. The Fermi energy is at zero.

from O atom, while the conduction band parts mainly arise from La and Zr atoms. The contribution of Li atom can be ignored. Therefore, there is a rather weak interaction between Li and La/Zr/O atoms, favorable for Li^+ migration in both t-LLZO and c-LLZO bulk structures.

3.2. Surface stability and electronic structure

3.2.1. Surface stability

Now, we turn to discuss the structural stability and electronic properties of LLZO surface. Surface properties of LLZO are important to the formation of lithium dendrites. In order to clarify the basic surface properties of LLZO, it is essential to construct the surface models firstly. The surface configurations with low Miller index are energetically stable for LLZO.[43–45] Therefore, we consider the (110) and (001) surfaces for both t- and c-LLZO in our calculations. Based on the stable bulk structure, several surface structures with different atomic terminations were constructed. The unrelaxed slab models of the (110) and (001) surfaces for t-LLZO are shown in Figs. S2 and S3, respectively, while the configurations for c-LLZO are shown in Figs. S4 and S5 in the supplementary material. Figure S2 shows that there are five types of terminations for the (110) surface in the t-LLZO, i.e., Li/La-, O1-, O2-, Zr-, and Li/O-ends. There are also five types of terminations for the (001) surface in the t-LLZO, i.e., Li/La-, Li-, O-, Zr-, and Li/O-ends as shown in Fig. S3. As shown in Fig. S4, there are four types of terminations for the (110) surface in the c-LLZO, i.e., Li/La-, Li-, O-, and Zr-ends. Figure S5 shows that there are only three types of terminations for the (001) surface in the c-LLZO, i.e., Li/La-, Li-, and O-ends. Herein, Li/La–T(110) represents the (110) surface of t-LLZO with Li/La-termination, Li/La–C(110) stands for the (110) surface of c-LLZO with Li/La-termination, and so on.

After obtaining the slab models, we will discuss their stability next. According to Eq. (1), the surface energies (γ_{surf}) for (110) and (001) facets with different terminations are summarized in Table 1. The relaxed slab structures for the energetically stable terminations are shown in Fig. 4. The calculated surface energies are reasonably in agreement with previous results.[44,45] Specifically, the surface energies are 1.02 $J{\cdot}m^{-2}$, 2.11 $J{\cdot}m^{-2}$, 2.24 $J{\cdot}m^{-2}$, 1.34 $J{\cdot}m^{-2}$, and 1.92 $J{\cdot}m^{-2}$ for the (110) surface of t-LLZO with Li/La-, O1-, O2-, Zr-, and Li/O-ends, respectively. The lowest surface energy of Li/La-termination implies that Li/La–T(110) is the most stable surface. In the Li/La–T(110) structure, we can see from Fig. 4(a) that the surface La atoms move towards the second layer perpendicular to the surface after relaxation. The surface energy values of the (110) surface of c-LLZO terminated with Li/La-, Li-, O-, and Zr-ends are 1.04 $J{\cdot}m^{-2}$, 0.86 $J{\cdot}m^{-2}$, 2.60 $J{\cdot}m^{-2}$, and 1.37 $J{\cdot}m^{-2}$, respectively, suggesting Li–C(110) surface is the most stable. After relaxation, the outmost Li-layer moves outwards, resulting into a larger distance between the outmost Li-layer and the second atomic layer in the Li–C(110) structure (Fig. 4(d)). For the (001) surfaces, Li/La- and Li-terminations are both thermodynamically stable due to the low surface energy. Moreover, Li-termination (0.88 $J{\cdot}m^{-2}$ for t-LLZO and 0.91 $J{\cdot}m^{-2}$ for c-LLZO) has a lower surface energy than Li/La-termination (0.98 $J{\cdot}m^{-2}$ for t-LLZO and 1.00 $J{\cdot}m^{-2}$ for c-LLZO). Figures 4(b), 4(c), 4(e), and 4(f) show that there are no prominent changes of the surface atomic configurations for the stable (001) surfaces after relaxation. In a word, for both (110) and (001) surfaces, the surface energies are close to or even less than 1.00 $J{\cdot}m^{-2}$ for Li/La- and Li-terminations, while slightly greater than 1.00 eV for Zr-termination, but significantly larger than 1.00 eV for O- and Li/O-terminations. This means that Zr-termination is more stable than O-rich termination but less stable than Li-rich termination for the (110) and (001) surfaces of both t-LLZO and c-LLZO. Therefore, the LLZO surfaces prefer to form the Li-rich surface structures. Hereafter the Li-rich surfaces are chosen for further investigations.

Table 1. Surface compositions (C_{surf}) and energies (γ_{surf}) of (110) and (001) surfaces with different terminations in the t-LLZO and the c-LLZO. The data of c-LLZO are shown in parentheses.

Facets	Termination	C_{surf}	γ_{surf} ($J{\cdot}m^{-2}$)
(110)	Li/La- (Li/La-)	$Li_{64}La_{28}Zr_{16}O_{96}$ ($Li_{75}La_{32}Zr_{24}O_{128}$)	1.02 (1.04)
	O1- (Li-)	$Li_{64}La_{28}Zr_{16}O_{112}$ ($Li_{64}La_{28}Zr_{16}O_{96}$)	2.11 (0.86)
	O2- (O-)	$Li_{64}La_{24}Zr_{24}O_{120}$ ($Li_{61}La_{24}Zr_{24}O_{120}$)	2.24 (2.60)
	Zr- (Zr-)	$Li_{56}La_{24}Zr_{24}O_{96}$ ($Li_{56}La_{24}Zr_{24}O_{96}$)	1.34 (1.37)
	Li/O-	$Li_{68}La_{24}Zr_{24}O_{120}$	1.92
(001)	Li/La- (Li/La-)	$Li_{48}La_{20}Zr_{12}O_{72}$ ($Li_{44}La_{20}Zr_{12}O_{72}$)	0.98 (1.00)
	Li- (Li-)	$Li_{56}La_{20}Zr_{12}O_{80}$ ($Li_{40}La_{16}Zr_{12}O_{64}$)	0.88 (0.91)
	O- (O-)	$Li_{56}La_{20}Zr_{12}O_{96}$ ($Li_{40}La_{16}Zr_{12}O_{72}$)	4.59 (2.24)
	Zr-	$Li_{56}La_{28}Zr_{20}O_{96}$	1.38
	Li/O-	$Li_{56}La_{20}Zr_{12}O_{88}$	2.62

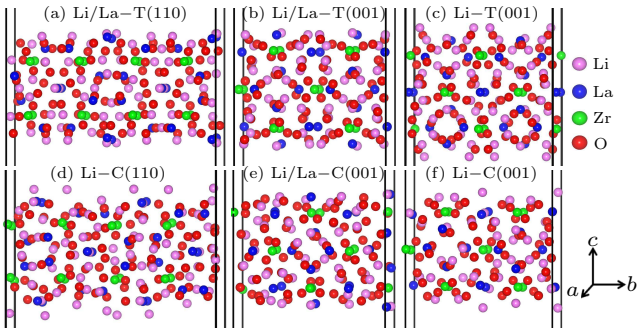


Fig. 4. The relaxed slab structures of the (110) and (001) surfaces with the low surface energies in the (a)–(c) t-LLZO and (d)–(f) c-LLZO.

As stated above, for either (110) surfaces or (001) surfaces, Li-rich surfaces show high stability, O-rich surfaces exhibit instability, and Zr-terminated surface lies in between. To better understand the different stability, we calculate the total and partial density of states (DOS) for the (110) and (001) surfaces with different terminations. There are similar results

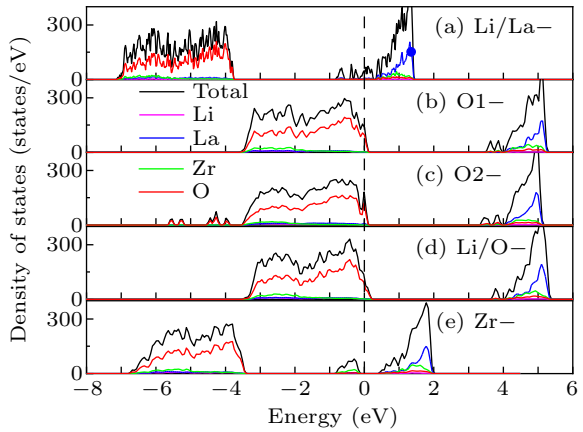


Fig. 5. Total and partial density of states for the (110) surfaces of t-LLZO with different terminations. The Fermi energy is at zero.

for the DOSs of the (110) and (001) surfaces. For simplicity, we only analyze the DOSs of t-LLZO (110) surfaces with various terminations, which are depicted in Fig. 5. Obviously, the electronic structures of the slab surfaces are closely related with the atom termination configurations, further affecting the surface energies. Comparing Figs. 5(a) and 5(e) makes us find that the Fermi level moves into the conduction band due to the excess Li/La atoms for the Li-rich surface, and its peaks shift to the lower energy region compared to Zr-terminated surface. In contrast, for the O-rich surfaces (Figs. 5(b)–5(d)), the Fermi level moves downward and then merges into the valence band. As a result, the peaks in the O-rich configurations shift to higher energy region than those in the Zr-terminated surface. Therefore, Zr-terminated surface shows higher stability than O-rich surface but lower stability than Li-rich surface.

3.2.2. Surface electronic structures

Another critical characteristic of surface structures is the electronic structure. For LLZO, Li/La–T(110), Li/La–T(001), Li–T(001), Li–C(110), Li/La–C(001), and Li–C(001) have been proved to be energetically favorable surfaces. Therefore, we mainly focus on analyzing the DOSs of these six surfaces. The calculated DOSs of isolated surface terminations in the six surfaces are presented in Fig. 6. Noticeably, LLZO bulk structures are all good insulators since the bandgaps are large (>4 eV) as shown in Fig. 3. However, Fig. 6 indicates that all of the stable LLZO surfaces become electronically conductive since some additional states exist in the bandgap. These new surface states in the bandgap tend to localize around the surface Li/La atoms, providing a possible electron pathway for metallic Li formation.

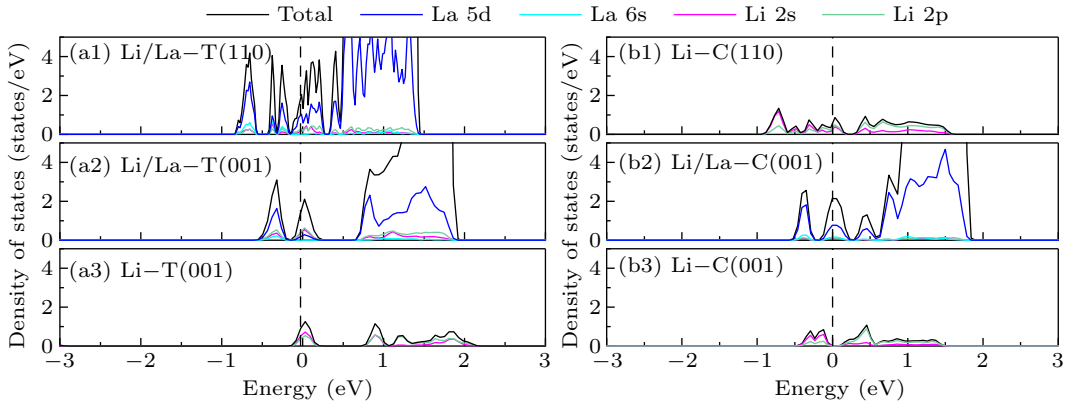


Fig. 6. Total and projected density of states of the top layer on the stable LLZO surfaces. Panel (a) for t-LLZO surfaces and panel (b) for c-LLZO surfaces. The Fermi energy is at zero.

3.3. The effect of Li concentration on the slab stability

Since the LLZO surfaces prefer the Li-rich surface structures as mentioned above, the agglomeration and deposition of Li atoms on the surface are easy to be formed, which would be benefit to the formation of Li dendrites of dead Li. To further explore the effect of Li concentration, we study the thermodynamic stability of the surface structures with varied Li concentration. Herein, the Li-rich configurations with the lowest surface energies are investigated for either t-LLZO or c-LLZO. For comparison, we consider both Li/La- and Li-terminated configurations for the (001) surface of t-LLZO. Specifically, for the t-LLZO, Li/La–T(110), Li/La–T(001), and Li–T(001) surfaces in Figs. 4(a)–4(c) are selected. For the c-LLZO, Li–C(110) and Li–C(001) surfaces in Figs. 4(d) and 4(f) are selected. We change the Li concentration by removing the Li-ions on the surfaces. The top and bottom surfaces are symmetrically changed. Therefore, two Li-ions are removed for every step. Figure 7 shows the surface energies as a function of the varied Li concentration on the surfaces. From this figure, some common features could be observed for either t-LLZO or c-LLZO. First, the surface energies decrease until one minimal value is attained with the decrease of Li-ions for either the (110) or (001) surfaces. Second, after reaching the minimal surface energy, the surface energies increase with the further decrease of Li-ions on the surfaces. That is to say, there is an opposite change trend for the surface energy before and after the minimum value.

Actually, there are two kinds of interaction for the out-

most Li atoms on the Li-rich LLZO surfaces, namely, the repulsive interaction between Li-ions in the top layer (named as Li–Li intralayer interaction) and the attractive interaction between Li-ions in the surface layer and O-ions in the next layer (named as Li–O interlayer interaction). The opposite variation trend for the surface energy before and after the minimum point may be attributed to the synergistic effect of the two interactions that is generally influenced by the Li contents. Before the minimum point, Li–Li intralayer interaction dominates over Li–O interlayer interaction. In this case, the Li-ions are easy to be removed from the surface due to the repulsive interaction between Li-ions, thus the surface energy gradually lowers with the decreased Li contents. Continuing to reduce Li-ions, the surface tends to have fewer Li-ions. In this case, Li–O interlayer interaction in turn is stronger than Li–Li intralayer interaction. As a result, in order to removing from the surface, the Li-ions must overcome the strong Li–O interlayer interaction, which induces an increased surface energy with decreased Li contents after the minimum point.

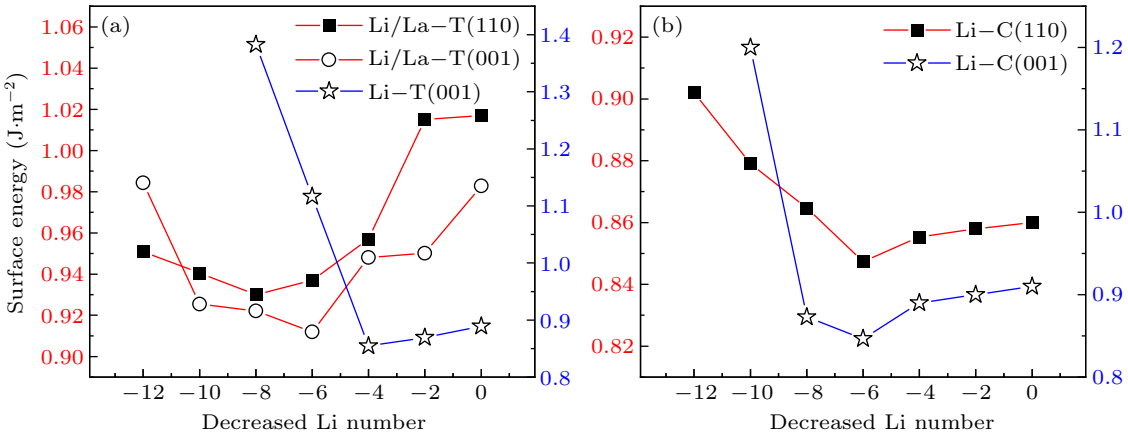


Fig. 7. Surface energy as a function of the varied Li concentration on the stable LLZO surfaces. Panel (a) for t-LLZO surfaces and panel (b) for c-LLZO surfaces.

3.4. The Li-ion transport at the LLZO surface

Li-ion transport characteristics on the surface play a vital role in the performance of SSEs. The conductivity of Li-ions could significantly affect the formation of the Li dendrites. In order to understand the growth mechanism of Li dendrites in LLZO SSEs, the migration properties of a single Li-ion on the surface were investigated. Meier *et al.*[29] had reported the mechanisms of Li diffusion in the t- and c-LLZO by the *ab-initio* molecular dynamics (AIMD) simulation methods. It was suggested that the motion of Li-ions is fully collective or synchronous for the bulk t-LLZO. The migration pathway is along with Li1 → Li3 → Li2 → Li3 → Li1 sites. The calculated barrier for Li-ion migration in the t-LLZO bulk is about 0.4 eV. We also calculate the barrier for Li-ion migration in bulk t-LLZO. The results are shown in Fig. 8. From Fig. 8, we can see that the migration barrier is 0.20 eV for Li1 → Li3 (path I) and 0.12 eV for Li3 → Li2 (path II). Clearly, for bulk t-LLZO, path II has the lower diffusion barrier compared to path I.

Owing to the Li-rich surface structures having the low surface energy and the Li distribution on the surface of the t-LLZO being more orderly, the (001) surfaces of t-LLZO with Li/La- and Li-terminations (Li/La–T(001) and Li–T(001)) are employed for the migration study. Similar to the migration in the bulk structures, the migration pathways of Li-ion on the surface are selected to be along Li1 → Li3 → Li2, as shown in Fig. 9(a), where the Li1 and Li2 sites are at the first layer, while the Li3 sites are at the second layer. Path I corresponds to the Li migration from Li1 to Li3 sites, and path II corresponds to the Li migration from Li3 to Li2 sites. In the Li/La–T(001) case, according to the CI-NEB results, the energy barrier of path I is only 0.08 eV (Fig. 9(b)), which is significantly lower than that in bulk LLZO.[29] As for path II, it is found that the Li at the Li3 site could spontaneously migrate to the adjacent Li2 site when the Li2 site on the surface is vacant. Therefore, compared to Li3 site, the Li-ions prefer to stay at the Li2 site on the surface.

However, the situation for the Li–T(001) surface is totally different. In this case, the Li3 sites lie at the first layer, while the Li1 and Li2 sites are at the second layer. Three migration pathways are considered for the Li–T(001) surface as given in Fig. 9(c). Similar to the case of the Li/La–T(001) surface, path I and path II correspond to the Li1 → Li3 and Li3 → Li2 pathways for the Li migration, respectively. Differently, path III represents the Li migration from Li3 site to the adjacent Li3 site. In addition to the pristine Li–T(001) surface, Li–T(001) surface with four Li vacancies is also used to investigate the Li diffusion. The diffusion barrier profiles for the three pathways on the Li–T(001) surfaces without and with Li vacancies are displayed in Figs. 9(d) and 9(e), respectively. For the pristine Li–T(001) surface (Fig. 9(d)), the energy barriers are calculated to be 0.74 eV, 0.50 eV, and 2.8 eV for path I, path

II, and path III, respectively. Obviously, path III shows the largest diffusion barrier, which surely hinders the diffusion of Li-ion within the same layer. In comparison, path I and path II possess relatively low diffusion barriers, which are however enormously larger than that in bulk and that in Li/La–T(001) surface. Therefore, it is not easy for the migration of Li-ion on the pristine Li–T(001) surface. Similar to the Li/La–T(001) surface, Li-ions on the Li–T(001) surface also tend to stay at the Li2 sites because path II has lower diffusion barrier than path I. From Fig. 7(a), we know that the Li–T(001) surface is the most stable when 4 Li-ions are removed from the pristine surface. In this case, the removal of Li atoms will produce Li vacancies on the surface. The as-formed Li vacancies may help the migration of Li-ion. To confirm this, we further calculate the migration barrier of Li-ion on the Li–T(001) surface with four Li vacancies. As expected, Fig. 9(e) shows that the diffusion barriers of Li-ion reduce from 0.74 eV to 0.70 eV for path I, while decrease from 0.50 eV to 0.34 eV for path II. Thus, by varying Li contents, we can obtain the Li–T(001) surface with higher stability and lower diffusion barrier. These advantages could inhibit the formation of metallic Li on the Li–T(001) surface.

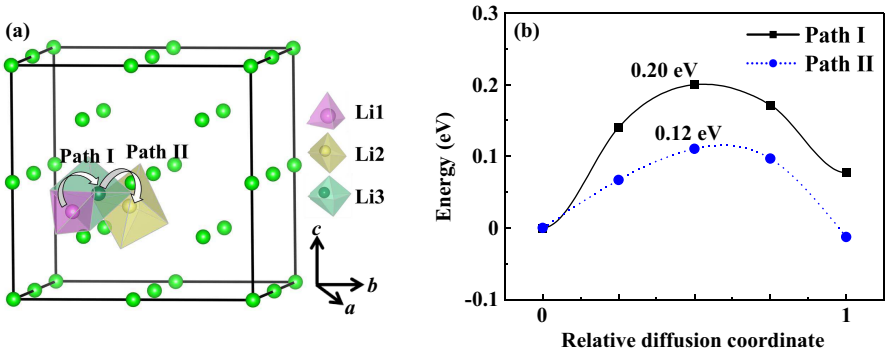


Fig. 8. Panels (a) and (b) are the migration pathways and the corresponding migration energy profiles in bulk t-LLZO.

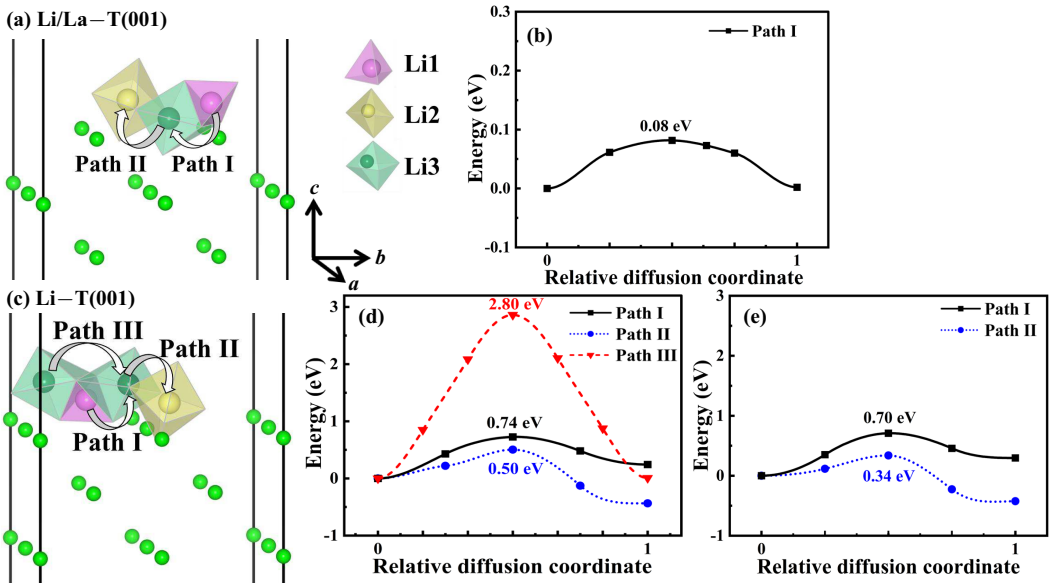


Fig. 9. Panels (a) and (c) are the migration pathways on the Li/La–T(001) and Li–T(001) surfaces, respectively. Panels (b), (d), and (e) are the corresponding migration energy profiles for Li/La–T(001), pristine Li–T(001), and Li–T(001) with four Li vacancies, respectively.

Based on our CI-NEB calculations, for bulk t-LLZO, Li/La–T(001) and Li–T(001) surfaces, path II (Li3 → Li2) shows the lowest diffusion barrier. In the same migration path, Li/La–T(001) surface has the lowest Li-ion migration barrier, Li–T(001) has the largest Li-ion migration barrier, and bulk t-LLZO lies in between. Therefore, the Li-ion migration on the Li/La–T(001) surface is much easier than that in bulk t-LLZO and on the Li–T(001) surface. It reveals that Li metal is easier to be formed on the Li-terminated surface. In addition, we find that the migration of Li-ions on the LLZO surfaces is closely related with the local structures of the surfaces. Although the Li/La–T(001) and Li–T(001) surfaces both belong to the Li-rich structure, the Li sites at the first layer are different, where Li1 and Li2 sites appear at the Li/La–T(001) surface but Li3 sites are at the Li–T(001) surface. The different distribution of Li sites on the surface layer leads to different Li–O bond strength. As shown in Table S1 in the supplementary material, the bond lengths of Li1–O, Li2–O, and Li3–O on the Li/La–

T(001) surface are all longer than those on the Li–T(001) surface, indicating weaker binding between Li and O atoms on the Li/La–T(001) surface. For this reason, Li-ions are easier to migrate on the Li/La–T(001) surface. Based on this, modification of the surface structures could be used to tune the migration of Li-ions at the surfaces, thus further affecting the formation of Li dendrites.

4. Conclusion

Several LLZO surface structures are investigated by the first-principles calculations to explore their stability, electronic and Li-ion mobility properties. It is found that for the (110) and (001) surfaces of t- and c-LLZO, Li-rich terminations are the energetically favorable slab structures. Further, with decreasing Li contents, the stability of Li-rich surfaces first enhances owing to the repulsive Li–Li intralayer interaction, and after the minimum point, the stability starts to drop markedly due to the attractive Li–O interlayer interaction. From the analysis of the DOSs, there are some localized surface states shown in the bandgap on the Li-rich surface structures of LLZO, but not in the bulk structures. These surface states provide a possible electron pathway for metallic Li formation on the Li-rich surface. Besides, we found that for the Li/La-terminated (001) surfaces of t-LLZO, Li-ion can spontaneously diffuse along path II (Li3 $\rightarrow$ Li2). Unfortunately, it is difficult for Li-ion diffusion on the Li-terminated (001) surface of t-LLZO. In this case, path III (Li3 $\rightarrow$ Li3) has the maximum diffusion barrier (2.80 eV), while path II (Li3 $\rightarrow$ Li2) possesses the minimum diffusion barrier (0.50 eV). In comparison, metallic Li can form more easily at the Li-end than at the Li/La-end. When reducing four Li atoms from the Li-terminated (001) surface of t-LLZO, the diffusion barrier for path II decreases to 0.34 eV, favorable for Li-ion diffusion. Clearly, for the Li-end, the stability and Li-ion diffusion barrier can be finely tuned by changing Li contents on the surface, thus further affecting the metallic Li formation. The present results enrich our understanding of Li dendrites growth on the LLZO surface.

Acknowledgment

Project supported by the National Natural Science Foundation of China (Grant Nos. 12064015 and 12064014).

References

[1] Armand M and Tarascon J M 2008 *Nature* **451** 652
[2] Feng X N, Ouyang M G, Liu X, Lu L G, Xia Y and He X M 2018 *Energy Stor. Mater.* **10** 246
[3] Goodenough J B and Park K S 2013 *J. Am. Chem. Soc.* **135** 1167
[4] Sun C W, Liu J, Gong Y D, Wilkinson D P and Zhang J J 2017 *Nano Energy* **33** 363
[5] Wang Y, Richards W D, Ong S P, Miara L J, Kim J C, Mo Y and Ceder G 2015 *Nat. Mater.* **14** 1026
[6] Goodenough J B and Kim Y 2009 *Chem. Mater.* **22** 587
[7] Aurbach D, Markovsky B, Salitra G, Markevich E, Talyossef Y, Koltypin M, Nazar L, Ellis B and Kovacheva D 2007 *J. Power Sources* **165** 491
[8] Swiderska-Mocek A, Lewandowski A and Kurc B 2011 *J. Solid State Electrochem.* **16** 673
[9] Chai M, Jin Y D, Fang S H, Yang L, Hirano S I and Tachibana K 2012 *Electrochim. Acta* **66** 67
[10] Mizuno F, Hayashi A, Tadanaga K and Tatsumisago M 2005 *Adv. Mater.* **17** 918
[11] Knauth P 2009 *Solid State Ion.* **180** 911
[12] Takada K 2013 *Acta Mater.* **61** 759
[13] Thompson T, Yu S, Williams L, Schmidt R D, Garcia-Mendez R, Wolfenstine J, Allen J L, Kioupakis E, Siegel D J and Sakamoto J 2017 *ACS Energy Lett.* **2** 462
[14] Thangadurai V, Narayanan S and Pinzaru D 2014 *Chem. Soc. Rev.* **43** 4714
[15] Wang C, Fu K, Kammampata S P, McOwen D W, Samson A J, Zhang L, Hitz G T, Nolan A M, Wachsman E D, Mo Y F, Thangadurai V and Hu L 2020 *Chem. Rev.* **120** 4257
[16] Murugan R, Thangadurai V and Weppner W 2007 *Angew. Chem. Int. Ed. Engl.* **46** 7778
[17] Wu B B, Wang S Y, Lochala J, Desrochers D, Liu B, Zhang W Q, Yang J H and Xiao J 2018 *Energy Environ. Sci.* **11** 1803
[18] Sharafi A, Haslam C G, Kerns R D, Wolfenstine J and Sakamoto J 2017 *J. Mater. Chem. A* **5** 21491
[19] Tsai C L, Roddatis V, Chandran C V, Ma Q, Uhlenbruck S, Bram M, Heitjans P and Guillon O 2016 *ACS Appl. Mater. Interfaces* **8** 10617
[20] Hongahally B R, Ito T, Morimura T, Bekarevich R, Mitsuishi K and Yamada H 2017 *J. Power Sources* **363** 145
[21] Wu J F, Pang W K, Peterson V K, Wei L and Guo X 2017 *ACS Appl. Mater. Interfaces* **9** 12461
[22] Zhuang L B, Huang X, Lu Y, Tang J W, Zhou Y J, Ao X, Yang Y and Tian B B 2021 *Ceram. Int.* **47** 22768
[23] Miara L J, Ong S P, Mo Y, Richards W D, Park Y, Lee J M, Lee H S and Ceder G 2013 *Chem. Mater.* **25** 3048
[24] Miara L J, Richards W D, Wang Y E and Ceder G 2015 *Chem. Mater.* **27** 4040
[25] Samson A J, Hofstetter K, Bag S and Thangadurai V 2019 *Energy Environ. Sci.* **12** 2957
[26] Ishiguro K, Nakata Y, Matsui M, Uechi I, Takeda Y, Yamamoto O and Imanishi N 2013 *J. Electrochem. Soc.* **160** A1690
[27] Garcia D F A, Bonilla M R, Llordes A, Carrasco J and Akhmatskaya E 2019 *ACS Appl. Mater. Interfaces* **11** 753
[28] Wang Y X, Huq A and Lai W 2014 *Solid State Ion.* **255** 39
[29] Meier K, Laino T and Curioni A 2014 *J. Phys. Chem. C* **118** 6668
[30] Xu M, Park M S, Lee J M, Kim T Y, Park Y S and Ma E 2012 *Phys. Rev. B* **85** 052301
[31] Kresse G and Furthmuller J 1996 *Phys. Rev. B* **54** 11169
[32] Kresse G and Joubert D 1999 *Phys. Rev. B* **59** 1758
[33] Perdew J P, Burke K and Ernzerhof M 1996 *Phys. Rev. Lett.* **77** 3865
[34] Perdew J P, Ernzerhof M and Burke K 1996 *J. Chem. Phys.* **105** 9982
[35] Monkhorst H J and Pack J D 1976 *Phys. Rev. B* **13** 5188
[36] Pack J D and Monkhorst H J 1977 *Phys. Rev. B* **16** 1748
[37] Henkelman G and Jónsson H 2000 *J. Chem. Phys.* **113** 9978
[38] Xu G, Zhong K, Zhang J M and Huang Z 2014 *J. Appl. Phys.* **116** 063703
[39] He B, Chi S T, Ye A J, Mi P H, Zhang L W, Pu B W, Zou Z Y, Ran Y B, Zhao Q, Wang D, Zhang W Q, Zhao J T, Adams S, Avdeev M and Shi S Q 2020 *Sci. Data* **7** 151
[40] Geiger C A, Alekseev E, Lazic B, Fisch M, Armbruster T, Langner R, Fechtelkord M, Kim N, Pettke T and Weppner W 2011 *Inorg. Chem.* **50** 1089
[41] Awaka J, Takashima A, Kataoka K, Kijima N, Idemoto Y and Akimoto J 2011 *Chem. Lett.* **40** 60
[42] Xie H, Alonso J A, Li Y T, Fernández-Díaz M T and Goodenough J B 2011 *Chem. Mater.* **23** 3587
[43] Canepa P, Dawson J A, Sai G G, Statham J M, Parker S C and Islam M S 2018 *Chem. Mater.* **30** 3019
[44] Tian H K, Xu B and Qi Y 2018 *J. Power Sources* **392** 79
[45] Gao B, Jalem R and Tateyama Y 2020 *ACS Appl. Mater. Interfaces* **12** 16350